第 36 卷第 3 期 无 机 化 学 学 报 Vol.36 No.3
2020 年 3 月 CHINESE JOURNAL OF INORGANIC CHEMISTRY 566-574

$g\text{-}C_3N_4/Ag/TiO_2$ 复合材料的构筑及其光催化性能

李 平# 张孝贤# 斯 颖 梁婷婷 刘 欢 邱灵芳 段舒祺 多树旺* 陈 忠
(江西科技师范大学材料与机电学院,江西省材料表面工程重点实验室,南昌 330013)

摘要: 以合成的 $g\text{-}C_3N_4$ 纳米片和 Ag/TiO_2 空心微球为原料,采用机械搅拌的方法构筑了 $g\text{-}C_3N_4/Ag/TiO_2$ 三元复合光催化剂。采用 X 射线衍射(XRD)、傅里叶变换红外光谱(FT-IR)、扫描电镜(SEM)、X 射线光电子能谱(XPS)、紫外-可见光漫反射(UV-Vis DRS)和光致发光光谱(PL)对 $g\text{-}C_3N_4/Ag/TiO_2$ 进行了表征。研究表明,$g\text{-}C_3N_4/Ag/TiO_2$ 是由 Ag/TiO_2 微球和 $g\text{-}C_3N_4$ 纳米片复合而成的。与 TiO_2 相比,其可见光响应范围延长,光生载流子的分离速率加快。在室温下,用降解罗丹明 B 的反应考察了 $g\text{-}C_3N_4/Ag/TiO_2$ 的可见光催化活性。研究表明,光照 180 min 时,$g\text{-}C_3N_4$(0.5%)$/Ag/TiO_2$ 显示了最高的光催化活性(91.9%),分别是 TiO_2 和 Ag/TiO_2 的 7.5 和 1.8 倍。光催化活性的提高与合理的异质结构建和 Ag 的导电性能有关。

关键词: 光催化; 二氧化钛; 模板法; 石墨相氮化碳; 罗丹明 B; 光降解
中图分类号: O614.41+1 **文献标识码**: A **文章编号**: 1001-4861(2020)03-0566-09
DOI:10.11862/CJIC.2020.055

Constructing and Photocatalytic Performance of $g\text{-}C_3N_4/Ag/TiO_2$ Composites

LI Ping# ZHANGA Xiao-Xian# SI Ying LIANG Ting-Ting LIU Huan
QIU Ling-Fang DUAN Shu-Qi DUO Shu-Wang* CHEN Zhong
(*Jiangxi Key Laboratory of Material Surface Engineering, School of Materials and Mechanical and Electrical Engineering, Jiangxi Science and Technology Normal University, Nanchang* 330013, *China*)

Abstract: $g\text{-}C_3N_4/Ag/TiO_2$ ternary photocatalysts were successfully constructed by a mechanical agitation method with as-synthesized Ag/TiO_2 hollow microspheres and $g\text{-}C_3N_4$ nanosheets as the raw materials. The photocatalysts were systematically characterized by X-ray diffraction (XRD), Fourier transform infrared spectroscopy (FT-IR), scanning electron microscopy (SEM), X-ray photoelectron spectroscopy (XPS), ultraviolet-visible diffuse reflectance spectroscopy (UV-Vis DRS), and photoluminescence spectra (PL). The results showed that $g\text{-}C_3N_4/Ag/TiO_2$ was assembled by Ag/TiO_2 microspheres and $g\text{-}C_3N_4$ nanosheets. Compared with TiO_2, the resultant $g\text{-}C_3N_4/Ag/TiO_2$ heterojunctions possessed longer visible-light response range and faster photo-induced carrier separation rate. At room temperature, the visible-light photocatalytic activity of $g\text{-}C_3N_4/Ag/TiO_2$ was investigated by photodegradation of rhodamine B (RhB). The results showed that the highest visible-light-driven photocatalytic efficiency of $g\text{-}C_3N_4$ (0.5%)$/Ag/TiO_2$ with 180 min of light irradiation was 91.9%, which was nearly 7.5 and 1.8 times higher than pure TiO_2 and two-component Ag/TiO_2, respectively. The enhanced photocatalytic activity could be mainly attributed to the reasonably designed heterojunctions and the electrical conductivity of Ag.

Keywords: photocatalysis; titanium dioxide; template method; rhodamine B; photodegradation

收稿日期:2019-10-30。收修改稿日期:2019-12-17。
国家自然科学基金(No.41763020)、江西省自然科学基金(No.20171BAB206008,20181BAB206011)、江西省教育厅科学技术研究项目(No.GJJ180635,GJJ180596,GJJ180603,GJJ170665)和江西科技师范大学博士启动基金(No.2017BSQD008)资助。
#共同第一作者。
*通信联系人。E-mail:swduo@imr.ac.cn

0 Introduction

With the increasing awareness of environmental issues and energy crisis, sunlight-driven photocatalysis has been extensively investigated as a potential strategy for environmental remediation and energy conversion[1-4]. Among the reported semiconductor photocatalysts, titanium dioxide (TiO_2) has received massive attention due to its advantage of low cost, safety and excellent stability[5-8]. Nevertheless, the photocatalytic efficiency of TiO_2 is inhibited significantly by the fatal drawback of wide band gap energy (~3.2 eV) and rapid recombination rate of photo-reduced e^--h^+ pairs in TiO_2 single-phase semiconductor[9-10]. Hence, it is significantly important to develop TiO_2-based photocatalysts by lowering the band gap and promoting the photoinduced electron-hole pairs separation[11]. Research today is mainly focused on developing high efficiency TiO_2-based photocatalysts by metal or non-metal doping, metal deposition, morphological control and formation of heterostructure with narrow band gap semiconductors[12-14].

Doping noble metal is considered to a key path to modify TiO_2[15]. Among of noble metals, Ag is received as a promising candidate as the electron mediators due to its relatively low cost, electrical conductivity and localized surface plasmon resonance (LSPR), which are helpful for extending visible light absorbance and promoting the photoinduced electron-hole pairs separation[16-17]. Another key point of constructing a highly efficient photocatalyst is to constructing heterostructure with narrow band gap semiconductors which is considered to a key path to increase the visible light response range and restrain photoreduced electron/hole pair recombination[3,17]. Among various types of semiconductors are capable of coupling with TiO_2, graphite-like carbon nitride (g-C_3N_4) is a suitable candidate due to its narrow band gap (~2.69 eV) and well-matched conduction band position with TiO_2. Many reported composites of TiO_2 and g-C_3N_4 indeed show higher performance than TiO_2[17-19]. Besides, the 2D structure of g-C_3N_4 also possesses other unique properties, such as easy fabricating heterojunctions with other semiconductors, easy availability, low cost. Moreover, combing 2D and 3D structure contributes to integrate their functionalities and tailor the single-component physicochemical properties[20]. Therefore, it is vital important to construct 3D/2D composite structure of Ag/TiO_2 hollow microspheres and g-C_3N_4 nanosheets with excellent visible-light photocatalytic performance.

In the present work, a novel composite of 3D Ag/TiO_2 hollow microspheres and 2D g-C_3N_4 nanosheets was successfully constructed via the template method and chemical reduction method, followed by a facile mechanical agitation method. The results demonstrated that g-C_3N_4 nanosheets allowed for the uniform distribution of Ag/TiO_2 microspheres leading to the increased contact areas. The as-obtained g-C_3N_4/Ag/TiO_2 photocatalyst showed excellent activity for photodegradation of rhodamine B (RhB) under visible light irradiation, which was nearly 7.5 and 1.8 times higher than pure TiO_2 and Ag/TiO_2. The possible mechanism for superior performance of as-obtained g-C_3N_4/Ag/TiO_2 was further analysed and proposed.

1 Experimental

1.1 Materials and characterization

Titanium(Ⅳ) isopropoxide (TIPT), silver nitrate ($AgNO_3$) polyvinylpyorrlidone (PVP) (M_W=30 000), melamine ($C_3H_6N_6$), trisodium citrate dihydrate ($Na_3C_6H_5O_7 \cdot 2H_2O$) and glucose were obtained commercially from Sinopharm Chemical Reagent Co., Ltd. Deionized water (DI) with a resistivity of 18.0 MΩ·cm was used in all experiments. All the reagents were analytically pure and used without further purification. Carbon microspheres were synthesized as reported in the literature[21-22]. The XRD patterns were collected on a XRD-6100 (Shimadzu, Japan) operated at 40 kV and 30 mA with a Cu $K\alpha$ X-ray radiation source, a nickel filter (λ=0.154 06 nm), and 2θ range of 10°~80°. The SEM images were received on a Sigma 300 (ZEISS, Germany) operated at 20 kV. FT-IR was measured on a VERTEX70 (Bruker, Germany), samples were compressed into disks with KBr and analyzed over the wavenumber range of 400~4 000 cm^{-1} with 100 scans

at a resolution of 4 cm^{-1}. UV-Vis DRS were measured with a UV-Vis Lambda 650s spectrophotometer (PerkinElmer, USA) using $BaSO_4$ as the reflectance standard. PL spectra were acquired on an Omni-PL (Zolix, China) spectrometer at room temperature using an excitation wavelength of 325 nm. XPS was performed on an ESCALAB 250Xi (ThermoFisher, USA), using Mg $K\alpha$ ($h\nu$=1 253.6 eV) as the excitation source.

1.2 Preparation of photocatalyst

1.2.1 Preparation of g-C_3N_4 nanosheets

g-C_3N_4 nanosheets were prepared according to reference[23]. Typically, g-C_3N_4 nanosheets were obtained by a two-step calcination thermal-etching method using melamine as precursor.

1.2.2 Preparation of TiO_2 hollow spheres

TiO_2 hollow spheres were synthesized via using carbon microspheres as template, as reported in a previous literature[24]. In a typical process, 0.3 g carbon microspheres were dispersed to 20 mL ethanol and stirred vigorously for 30 min, and then another solution containing 3 mL of TIPT and 20 mL of ethanol was added dropwise into the above solution under stirring. Subsequently, the mixture was then transferred to a 100 mL Teflon-lined stainless steel autoclave and heated at 180 ℃ for 24 h. After cooling down to room temperature, the brown product was collected and washed with water and ethanol by centrifugation, and then dried at 60 ℃ for 12 h. Finally, the white TiO_2 hollow spheres were obtained by calcined at 450 ℃ in air for 3 h.

1.2.3 Preparation of Ag/TiO_2 composites

Ag-loaded TiO_2 (Ag/TiO_2) was synthesized through using sodium citrate as reductant. In a typical synthesis, 7.99 g TiO_2 and 1.0 g PVP were dispersed to 80 mL water and stirred for 30 min. Then another 20 mL aqueous solution containing 0.169 g $AgNO_3$ and 0.3 g sodium citrate was added with drop by drop to the above solution under stirring. Next, the mixture solution was stirred and maintained at 100 ℃ for 1 h. After cooling down to room temperature, the product was collected and washed thoroughly with water and ethanol by centrifugation, and then dried at 60 ℃ for 12 h.

1.2.4 Preparation of g-C_3N_4/Ag/TiO_2 photocatalysts

The g-C_3N_4/Ag/TiO_2 composite photocatalysts were successfully constructed via mechanical agitation method. Typically, 0.1 g Ag/TiO_2 and 0.005 g g-C_3N_4 nanosheets were dispersed in 60 mL absolute alcohol via ultra-sonication for 2 h, followed by mechanical stirring for 48 h. Finally, the product was washed with ethanol by centrifugation, and then dried at 60 ℃ for 12 h. Other composites with different weight percentages of g-C_3N_4 (1% and 3%) were obtained via the same procedure. For comparison, g-C_3N_4 (0.5%)/TiO_2 composite with weight percent of 0.5% was prepared via the same procedure without the depositing process of Ag.

1.3 Measurement of photocatlytic performance

Photocatalytic performance of the samples for removal of RhB was evaluated within an optical reaction apparatus (XPA Xujiang, China) under visible-light irradiation. Before illumination, the mixture was continuously stirred for 90 min in the dark to achieve the adsorption-desorption equilibrium between RhB and the samples. Then a 500 W Xe lamp (with 420 nm UV-cutoff filter) was turned on, the samples was extracted at 20 min intervals and separated by centrifugation for analysis. The concentration (C) of RhB was measured from the peak intensity at the maximal absorption wavelength using a Hitachi U-3010 UV-Vis spectrophotometer. The ratio (C/C_0) was adopted to determine the photocatalytic performance.

2 Results and discussion

2.1 Crystal structure

The crystalline phase of all samples was analysed by XRD, as shown in Fig.1a. The two diffraction peaks located at around 2θ=13.0° and 27.4° corresponded to the (100) and (002) reflection planes of pure g-C_3N_4 (PDF No.87-1526), The diffraction peaks of pristine TiO_2 at 25.3°, 37.8°, 48.1°, 54.1°, 54.9°, 62.7°, 68.9°, 70.3°, and 75.1° can be well assigned to the (101), (004), (200), (105), (211), (204), (116), (220) and (215) reflection planes of anatase TiO_2 (PDF No.21-1272), respectively. Nevertheless, the diffraction peak intensity corresponding to g-C_3N_4 and Ag was weak and inconspicuous in the binary and ternary

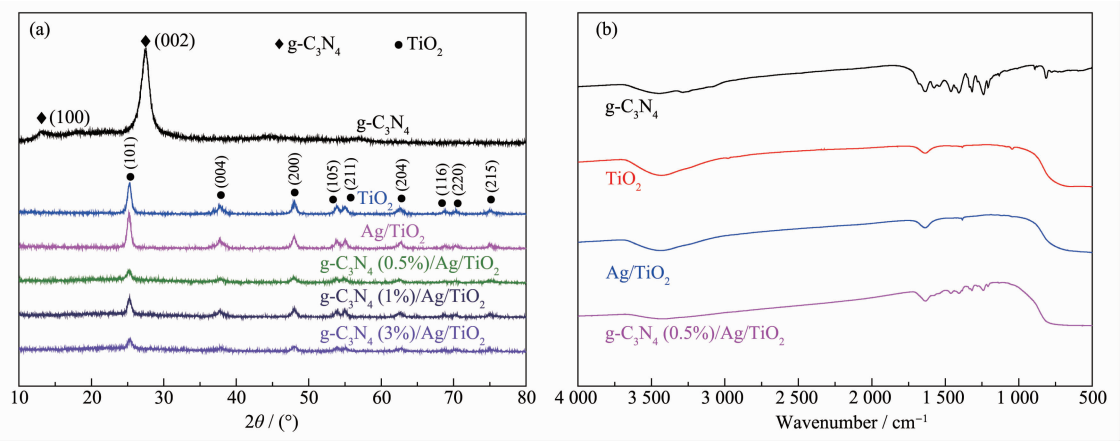

Fig.1　(a) XRD patterns and (b) FT-IR spectra of as-synthesized samples

composites, which can be attributed to the relatively low concentration or high dispersion in the samples[17]. Moreover, it can be seen that there was no impurity formed during the synthesis process of composites photocatalysts.

The FT-IR technique was used to analyse functional groups as displayed in Fig.1b. For pure g-C_3N_4, the obvious signals located at 1 200~1 600 cm^{-1} region could be ascribed to the C-N and aromatic C-N heterocycles stretching vibration modes[25-26]. Besides, the signal located at 808 cm^{-1} corresponded to typical breathing mode of tris-triazine rings. With regard to pure TiO_2, the characteristic signal located at 500~800 cm^{-1} corresponded to Ti-O-Ti and Ti-O stretching vibration modes, and the signals at 1 650 and 3 400~3 500 cm^{-1} regions were ascribed to the O-H group and absorbed water[27]. For g-C_3N_4 (0.5%)/Ag/TiO_2 composite, all signals of g-C_3N_4 and TiO_2 were observed obviously. Along with XRD results, the FT-IR test confirms that the structures of both g-C_3N_4 and TiO_2 were well kept in the ternary composite.

2.2　Morphology characterizations

Fig.2 shows SEM images of carbon spheres, pristine g-C_3N_4 nanosheets, TiO_2, Ag/TiO_2 and g-C_3N_4

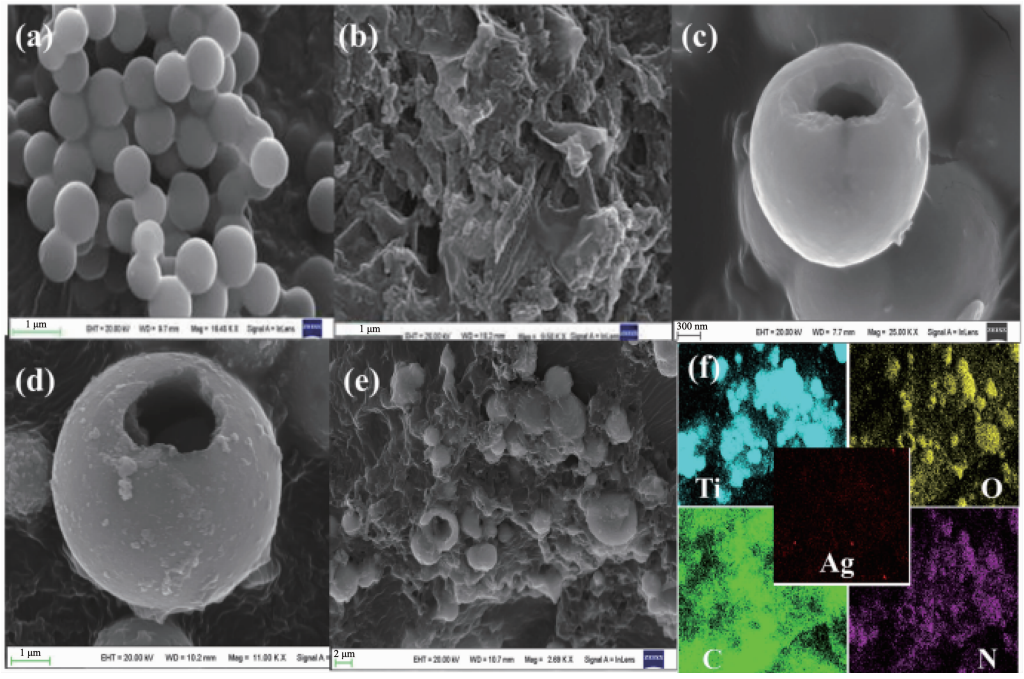

Fig.2　SEM images of (a) carbon spheres, (b) g-C_3N_4, (c) TiO_2, (d) Ag/TiO_2, (e) g-C_3N_4 (0.5%)/Ag/TiO_2; (f) EDS elemental mappings of g-C_3N_4 (0.5%)/Ag/TiO_2

(0.5%)/Ag/TiO_2. The diameter of carbon spheres could be estimated to be 400~500 nm from Fig.2a. As shown in Fig.2b, the pristine g-C_3N_4 exhibited irregular and loose agglomeration characteristic of curly nanosheets. In contrast, the TiO_2 sample displayed regularly hollow microsphere structure (Fig.2c). After combining TiO_2 with Ag, the Ag uniformly distributed on the surface of TiO_2 hollow microsphere (Fig.2d). Further, after combining Ag/TiO_2 and g-C_3N_4, the Ag/TiO_2 hollow spheres were equably attached to surface of g-C_3N_4 nanosheets (Fig.2e), this interaction can contribute to promote the photo-generated charge transfer and separation, and then increase photocatalytic activity. Energy dispersive X-ray spectroscopy (EDS, Fig.2f) analysis of g-C_3N_4 (0.5%)/Ag/TiO_2 further confirms that the ternary composite mainly consisted of Ti, O, C, N, and Ag elements, which indicates the successful fabrication of the target product. Furthermore, the EDS results show that the molar ratio of Ti, O, C, N, and Ag elements in g-C_3N_4 (0.5%)/Ag/TiO_2 were about 1.20:2.40:0.024:0.032:0.009, which in good agreement with that of starting materials.

2.3 XPS analysis

XPS spectra of as-obtained g-C_3N_4 (0.5%)/Ag/TiO_2 were used to notarize the chemical composition and status of elements, as shown in Fig.3. Fig.3a exhibits the XPS survey spectrum of the sample, suggesting that the sample was consisted of Ag, C, N, Ti and O

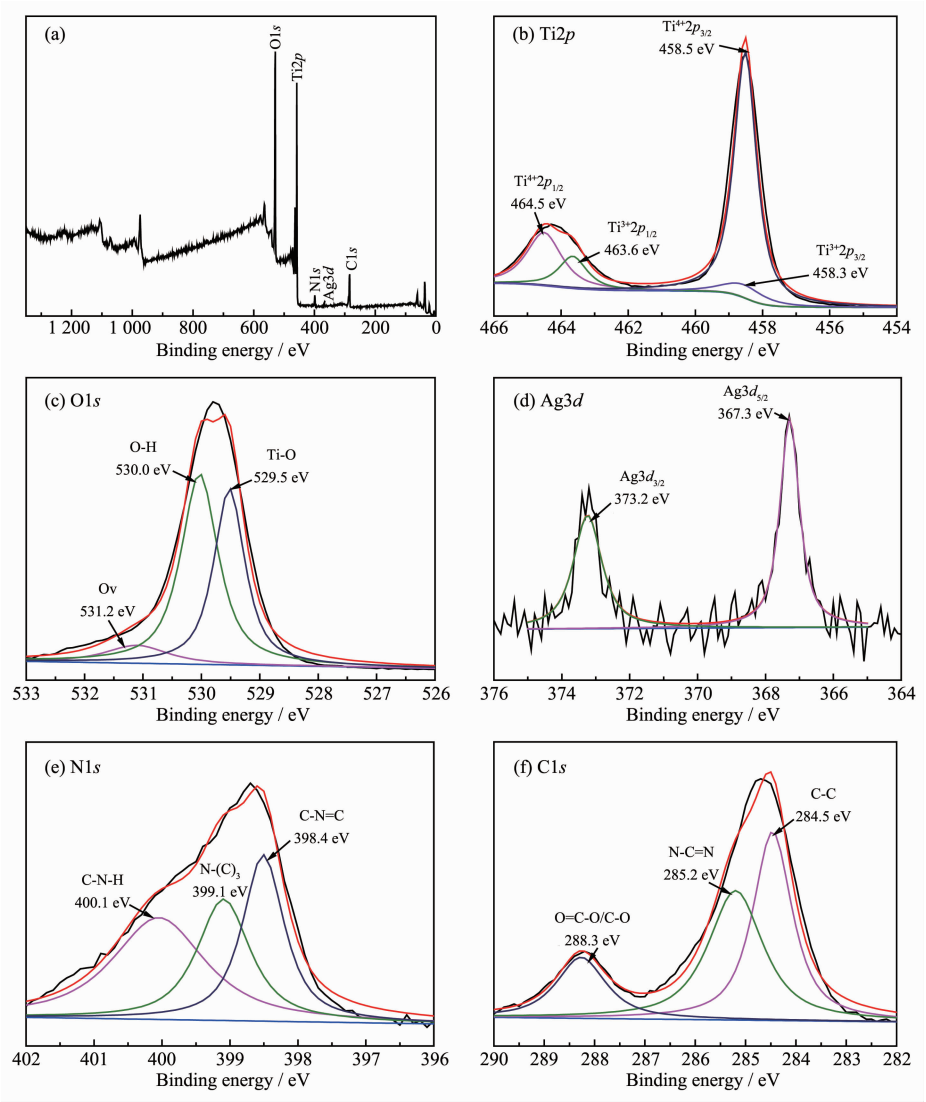

Fig.3 (a) XPS survey spectrum of g-C_3N_4(0.5%)/Ag/TiO_2; High-resolution spectra of (b) Ti2*p*, (c) O1*s*, (d) Ag3*d*, (e) N1*s*, and (f) C1*s* for g-C_3N_4 (0.5%)/Ag/TiO_2

elements. Fig.3b displays the XPS spectrum of Ti2*p*, which was consisted of four peaks at 464.5, 463.6, 458.5 and 458.3 eV. The binding energies at 464.5 and 458.5 eV could be ascribed to the $2p_{1/2}$ and $2p_{3/2}$ of Ti^{4+} orbitals, respectively[28]. While the electron binding energies at 463.6 and 458.3 eV corresponded to the $2p_{1/2}$ and $2p_{3/2}$ of Ti^{3+} orbitals, respectively[29]. The results indicate the coexistence of Ti^{4+} and Ti^{3+} species in the sample. In Fig.3c, the XPS spectrum of O1*s* was fitted into three peaks at 531.2, 530.0 and 529.5 eV, which could be ascribed to the oxygen vacancy (Ov), hydrogen oxygen bond (O-H) and titanium oxygen bond (Ti-O) respectively. The Ov indicated the exist of Ti^{3+}[30]. For the XPS spectrum of Ag3*d* (Fig.3d), two independent peaks at 373.3 and 367.3 eV could be ascribed to Ag3$d_{3/2}$ and 3$d_{5/2}$, respectively, suggesting the characteristic of metallic silver[30-31]. Fig.3e reveals the XPS spectrum of N1*s* with three peaks centered at 400.1, 399.1 and 398.4 eV, which could be ascribed to the sp^2-hybridized N bound to carbon atom (C-N=C), tertiary nitrogen N-$(C)_3$ and C-N-H groups[32], respectively. With regard to C1*s*, the XPS spectrum (Fig.3f) can be divided into three peaks of 288.3, 285.2 and 284.5 eV. The binding energies at 284.5 and 285.2 eV can be assigned to the sp^2 C-C bonds and sp^2-bonded C in N-C=N of g-C_3N_4[33], and the peak at 288.3 eV corresponded to the O=C-O or C-O bond in the skeleton[28].

2.4 PL spectra

The PL spectra are adopted to further investigate the separation difference of the photo-induced charge carriers. As shown in Fig.4, pristine TiO_2 presented high PL intensity, which is mainly attributed to quick photon-generated e^--h^+ pairs recombination rate, but after introducing Ag, the PL intensity decreased slightly. Furthermore, The PL intensity of g-C_3N_4 (0.5%)/Ag/TiO_2 decreased remarkably, which was much lower than that of pristine TiO_2, implying that high separation efficiency of photo-induced charge carriers existed in the ternary photocatalyst, which always associated with the enhanced photocatalytic activity.

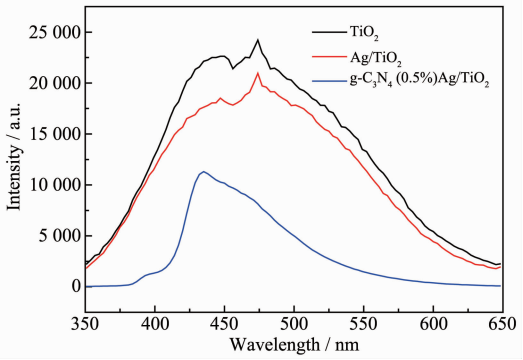

Fig.4　PL spectra of as-prepared samples

2.5 Optical absorption behaviour

The UV-Vis DRS of as-prepared samples was performed to assess the optical absorbance properties and bandgap. As shown in Fig.5a, pure g-C_3N_4 possessed an absorption edge at about 451 nm, while the absorption edge of TiO_2 appeared at 381 nm. Compared with TiO_2, the absorption edge of Ag/TiO_2 composite had a slightly red-shift, which may be partly ascribed to the interaction of TiO_2 and Ag nanoparticles. Furthermore, g-C_3N_4 (0.5%)/Ag/TiO_2 showed wider adsorption range than Ag/TiO_2 as a result of the incorporating g-C_3N_4 with relatively narrower bandgap. Besides, the values

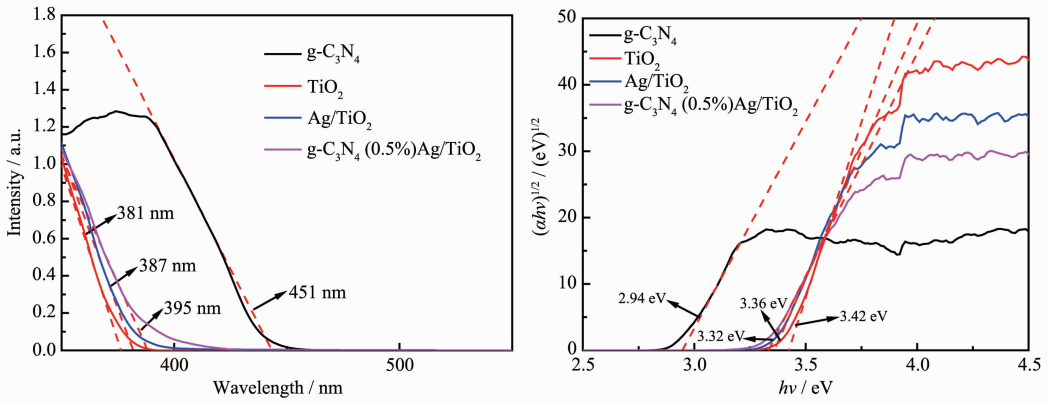

Fig.5　(a) UV-Vis DRS and (b) computation of the indirect interband transition energies of as-prepared samples

of band gap energies can be calculated according to the Tauc plot (where α, h, ν are the absorption coefficient, Planck constant and light frequency, respectively). As demonstrated in Fig.5b, the E_g of g-C_3N_4, TiO_2, Ag/TiO_2, g-C_3N_4 (0.5%)/Ag/TiO_2 can be calculated as 2.94, 3.42, 3.36 and 3.32 eV, respectively. The results indicate that g-C_3N_4 (0.5%)/Ag/TiO_2 sample displayed enhanced light harvesting ability compared with TiO_2 and Ag/TiO_2, which is a vital aspect to improve photocatalytic activity.

2.6 Photocatalytic performance

The photocatalytic degradation of RhB (10 mg·L^{-1}) in solution under visible-light illumination using no catalyst, pure g-C_3N_4 nanosheets, pristine TiO_2, Ag/TiO_2 and g-C_3N_4 (0.5%)/Ag/TiO_2 with different concentration of g-C_3N_4 as photocatalysts was measured to verify the enhanced photodegradation efficiency. As shown in Fig.6a, the concentration of RhB did not show obvious change in absence of catalyst. Pure g-C_3N_4 nanosheets showed relatively ideal photocatalytic effect. In contrast, pristine TiO_2 exhibited weak photodegradation efficiency of RhB under visible-light irradiation. However, the photocatalytic activity of g-C_3N_4 (0.5%)/TiO_2 and Ag/TiO_2 two-component composites were obviously enhanced compared with that of pristine TiO_2, which iwas attributed to the formation of heterojunction with g-C_3N_4 and good conductivity of Ag, respectively. Furthermore, when coupling TiO_2/Ag with g-C_3N_4, the degradation efficiency of RhB became much higher than that of two-component composites. Especially, when the load ratio of g-C_3N_4 was 0.5%, the degradation efficiency became 91.9%, which was 79.9% higher than using pristine TiO_2 and 41.7% higher than using Ag/TiO_2, respectively.

The photocatalytic reusability of g-C_3N_4 (0.5%)/Ag/TiO_2 was further evaluated by photodegradation of RhB under visible light cycled for four times. As shown in Fig.6b, the photocatalytic efficiency of g-C_3N_4 (0.5%)/Ag/TiO_2 sample for RhB degradation decreased from 91.9%% to 79.6% after four cycling runs, which showed that the g-C_3N_4 (0.5%)/Ag/TiO_2 sample can maintain relative good reusability in the photocatalytic degradation process under visible-light irradiation.

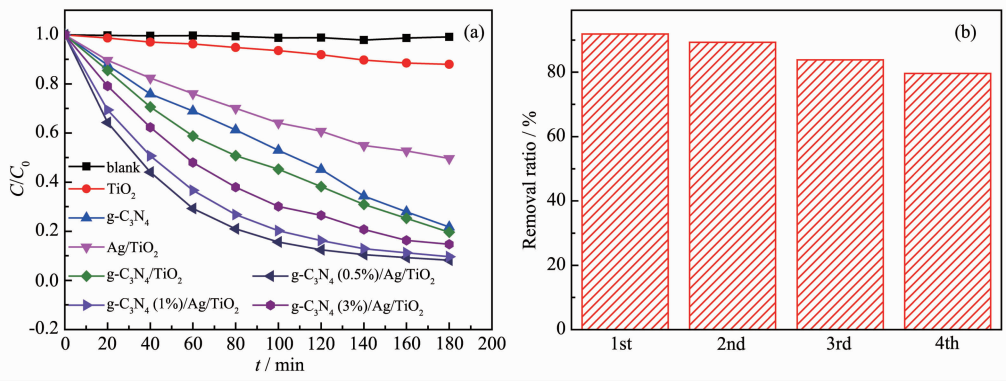

Fig.6 (a) Photocatalytic degradation of RhB under visible light irradiation; (b) Cycling runs of g-C_3N_4 (0.5%)/Ag/TiO_2 sample

2.7 Photocatalytic performance enhancement mechanism

To elucidate the photocatalytic performance degradation mechanism, isopropanol (IPA), 1,4-benzoquinone (BQ) and EDTA-2Na were adopted as hydroxyl free radicals (·OH), superoxide radical ($\cdot O_2^-$) and photogenerated holes (h^+) scavenger in RhB degradation system over g-C_3N_4 (0.5%)/Ag/TiO_2, respectively. As shown in Fig.7, the photodegradation rate of RhB showed no obvious decrease with the addition of IPA indicating that ·OH made no contribution to the photocatalytic activity. While declined photodegradation rates were observed in the presence of EDTA-2Na and BQ. Therefore, it is not difficult to deduce that h^+ and $\cdot O_2^-$ are the crucial active species during the photocatalytic process.

Based on above analysis, the probable photocatalytic activity enhancement mechanism for the charge transfer of g-C_3N_4 (0.5%)/Ag/TiO_2 was proposed. As show in Fig.8a, g-C_3N_4 can easily adsorb photons and

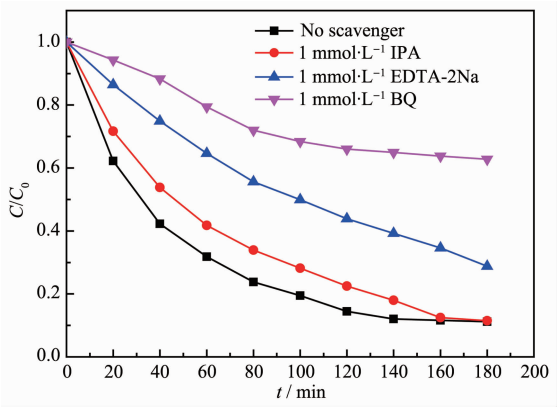

Fig.7　RhB degradation over g-C_3N_4 (0.5%)/Ag/TiO_2 in the presence of different scavengers

generate e^--h^+ pairs under visible-light irradiation. Since both the conduction band (CB) and valence band (VB) g-C_3N_4 were lower than those of TiO_2[34], the photo-generated electrons of g-C_3N_4 migrated to the surface of TiO_2. Furthermore, Ag can serve as a bridge for electron transfer between TiO_2 and g-C_3N_4, the excited state electrons at the of g-C_3N_4 could easily transfer to that of TiO_2. Subsequently, the electrons in CB of TiO_2 can be trapped by molecular oxygen dissolved in the solution to produce active species $\cdot O_2^-$. The obtained $\cdot O_2^-$ and h^+ stay in the VB of g-C_3N_4, and can directly react with RhB adsorbed on the surface of samples due to their high oxidative capacity. In addition to the enhanced charge separation, the hollow structure of TiO_2 may have some benecial effects on the photocatalytic performance. On the one hand, the hollow structure can allow more exposure surface to act as oxidation reaction active sites. On the other hand, the hollow structure promotes multiple reflections of light in the cavity leading to enhance the light harvesting. The possible light path in the cavity is shown in Fig.8b. Therefore, the enhancement of photocatalytic activity is mainly attributed to the effective separation efficiency of carriers and TiO_2 hollow sphere structure.

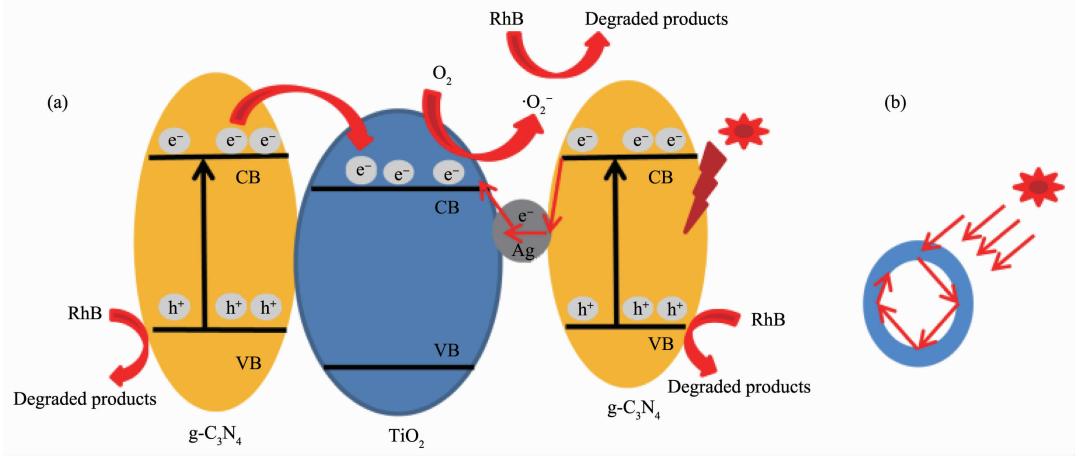

Fig.8　(a) Possible charge carriers separation and transfer mechanism; (b) Scheme of light path in the TiO_2 hollow microsphere

3　Conclusions

In summary, 3D Ag/TiO_2 hollow microspheres coupled with 2D g-C_3N_4 nanosheet as heterojunctions were successfully constructed by a simple mechanical agitation method. The as-synthesised ternary composites loaded with 1% Ag and 0.5% g-C_3N_4 nanosheets exhibited the highest photodegradation performance under visible-light irradiation. The enhanced visible light photocatalytic activity mainly contributed to promoting the separation of charge carriers by the synergistic effect of the formation of heterojunction with g-C_3N_4 and the good conductivity of Ag, moreover, enhancing effectively the utilization efficiency of the visible light by constructing TiO_2 hollow sphere structure. The study will provide a promising insight for constructing visible-light-driven photocatalyst for environmental remediation.

Acknowledgements: This work was supported by the National Natural Science Foundation of China (Grant No. 41760300), Natural Science Foundation of Jiangxi Province

(Grant No.20171BAB206008, 20181BAB206011), Scientific Research Fund of Jiangxi Provincial Education Department (Grant No.GJJ180635, GJJ180596, GJJ180603, GJJ170665) and the Doctoral Research Foundation of Jiangxi Science and Technology Normal University (Grant No.2017BSQD008).

References:

[1] You Z Y, Wu C Y, Shen Q H, et al. *Dalton Trans.*, **2018**,**47**: 7353-7361

[2] Cao Y, Xing Z P, Li Z Z, et al. *J. Hazard. Mater.*, **2018**,**343**: 181-190

[3] Qi K Z, Cheng B, Yu J G, et al. *Chin. J. Catal.*, **2017**,**38**: 1936-1955

[4] JIANG Hai-Yan(蒋海燕), ZHANG Fan(张 钒), YU Shu-Guang(于曙光), et al. *Chinese J. Inorg. Chem.*(无机化学学报), **2019**,**35**:695-702

[5] Kment S, Riboni F, Pausova S, et al. *Chem. Soc. Rev.*, **2017**, **46**:3716-3769

[6] Schipper D E, Zhao Z, Leitner A P, et al. *ACS Nano*, **2017**, **11**:4051-4059

[7] Lu D Z, Fang P F, Wu W H, et al. *Nanoscale*, **2017**,**9**:3231-3245

[8] Zhou W, Li W, Wang J Q, et al. *J. Am. Chem. Soc.*, **2014**, **136**:9280-9283

[9] Zeng M, Li Y Z, Mao M Y, et al. *ACS Catal.*, **2015**,**5**:3278-3286

[10]Zhou J, Luo P, Sun C, et al. *Nanoscale*, **2017**,**9**:4244-4254

[11]Chong B H, Zhu W, Hou X H. *J. Mater. Chem. A*, **2017**,**5**: 6233-6244

[12]Yang N, Li G Q, Wang W L, et al. *J. Phys. Chem. Solids*, **2011**,**72**:1319-1324

[13]Shao J, Sheng W C, Wang M S, et al. *Appl. Catal. B*, **2017**, **209**:311-319

[14]Wang Y Z, Duan S Y, Tian Z F, et al. *J. Mater. Chem. A*, **2017**,**5**:6047-6051

[15]Zhou P, Yu J G, Jaroniec M. *Adv. Mater.*, **2014**,**26**:4920-4935

[16]Wang J, Zhang W D. *Electrochim. Acta*, **2012**,**71**:10-16

[17]Zou Y J, Shi J W, Ma D D, et al. *ChemCatChem*, **2017**,**9**: 3752-3761

[18]Liu Y, Zeng X K, Hu X Y, et al. *Catal. Today*, **2019**,**335**: 243-251

[19]Zhou J, Wu H, Sun C Y, et al. *J. Mater. Chem. A*, **2018**,**6**: 21596-21604

[20]Chen Q F, Ren B S, Zhao Y B, et al. *Chem. Eur. J.*, **2014**, **20**:17039-17046

[21]Lan S, Liu L, Li R Q, et al. *Ind. Eng. Chem. Res.*, **2014**,**53**: 3131-3139

[22]Xi J B, Sun H Y, Wang D, et al. *Appl. Catal. B*, **2018**,**225**: 291-297

[23]Xu Q L, Zhu B C, Jiang C J, et al. *Solar RRL*, **2018**,**2**: 1800006

[24]Wang W K, Xu D F, Cheng B, et al. *J. Mater. Chem. A*, **2017**,**5**:5020-5029

[25]Shen L Y, Xing Z P, Zou J L, et al. *Sci. Rep.*, **2017**,**7**:41978-41984

[26]Zhang L Q, He X, Xu X W, et al. *Appl. Catal. B*, **2017**,**203**: 1-8

[27]Niu P, Zhang L L, Liu G, et al. *Adv. Funct. Mater.*, **2012**, **22**:4763-4770

[28]Yang K, Meng C, Lin L L, et al. *Catal. Sci. Technol.*, **2016**, **6**:829-839

[29]Zhidkov I S, McLeod J A, Kurmaev E Z, et al. *Appl. Phys. Lett.*, **2016**,**109**:022108

[30]Yu D H, Yu X D, Wang C H, et al. *ACS Appl. Mater. Interfaces*, **2012**,**4**:2781-2787

[31]Lei Y, Mehmood F, Lee S, et al. *Science*, **2010**,**328**:224-228

[32]He T, Wang L B, Santiago F F, et al. *J. Mater. Chem. A*, **2017**,**5**:6455-6464

[33]Jiang W, Liu H Z, Yin L, et al. *J. Mater. Chem. A*, **2013**,**1**: 6433-6440

[34]Chen Y F, Huang W X, He D L, et al. *ACS Appl. Mater. Interfaces*, **2014**,**6**:14405-14414